Modeling Artificial Molecules Composed of Coupled Quantum Dots*

Richard Akis and Dragica Vasileska

Department of Electrical Engineering, Arizona State University
Tempe, AZ 85287-5706, USA
richard.akis@asu.edu, vasilesk@imap2.asu.edu

ABSTRACT

Recently, there has been much interest in coupled quantum dots. With individual dots, if the energy levels can be resolved, then one can think of a dot as representing an "artificial atom" [1]. Thus, fabricating multiple quantum dots by using a split metal gate pattern over a GaAs-AlGaAs heterostructure, and allowing the dots to couple via quantum point contacts (QPCs), provides a way of creating "artificial molecules"[2]. Modeling such structures using a finite difference approach, we obtain the self-consistent confining potentials that are used in a 2-dimensional Schrödinger solver. The eigenstates of the resulting coupled systems show hybridization effects analogous to that of true molecules. Moreover, many of the eigenstates of these systems show evidence of wave function scarring, a phenomenon where the probability amplitude of the eigenstate is maximized along the path of a classical trajectory.

Keywords: quantum dots, heterostructures, mesoscopic, chaos, periodic orbits.

1. INTRODUCTION

In this paper, we show how one can calculate the confining potentials and compute the eigenstates for coupled quantum dot systems, which have been thought of as being analogous to molecules. We examine the physics of these systems closely, demonstrating just how close the molecular analogy follows. Not only do we see "molecular" behavior, we also see an effect known as "scarring", which indicates that classical electron trajectories play an important role in determining the quantum mechanical eigenstates. Our results have important implications, as they show that there is no simple crossover from "atomic" to "molecular" regimes, something that has been taking for granted in previous work on these structures.

2. METHOD

Experimentally, quantum dots can be realized by appliying metal gates over a GaAs/$Al_xGa_{1-x}As$ heterostructure using standard lithographic techniques. The gate pattern we have chosen to simulate is shown in the top panel of Fig. 1. As is evident, there are actually a number of gates, each of which can be controlled independently. The two center gates have been highlighted by shading them gray. In the calculations shown in section 5, it is these gates that are varied in voltage, while all the other gates are fixed at a voltage of *–1.0 V*.

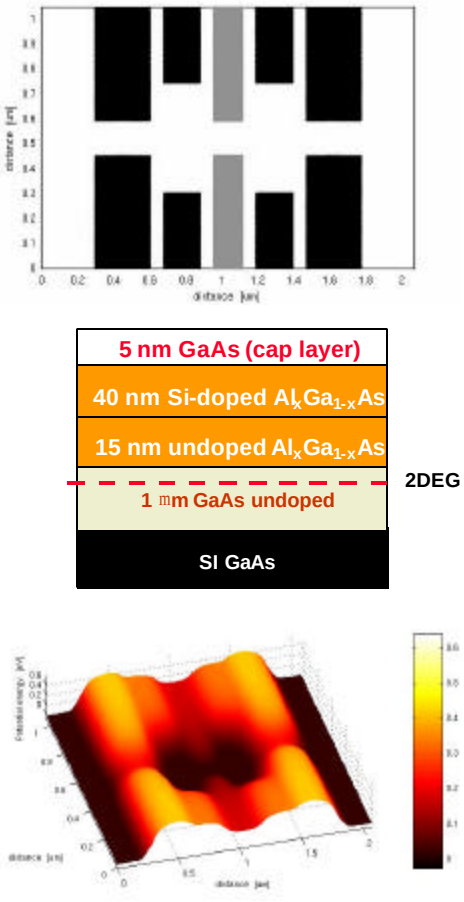

Figure 1: Upper panel: the gate pattern, middle panel: the heterostructure, lower panel: the confining potential given V_c = *-0.6V*.

The heterostructure we have simulated is shown in the middle panel of Fig. 1. It consists of a 5 nm undoped GaAs cap layer, a 40 nm $Al_xGa_{1-x}As$ (x=0.26) Si-doped ($N_D=1.5\times10^{18}$ cm^{-3}) barrier layer, and a 15 nm undoped

$Al_xGa_{1-x}As$ spacer layer, atop the GaAs substrate, in which the 2 dimensional electron gas (2DEG) forms (this is indicated by the dashed line). Finding the self-consistent solutions for the potential requires solving the 3D-Poisson equation, solving the 1D-Schrödinger equation and reconciling the potential and electron density in an outer iteration for self-consistency [3]. The bottom panel of Fig. 1 shows the potential slice $V(x,y,z_o)$, where z_o corresponds to the position of the centroid of the 2DEG along the z-axis. It is this potential that is used as the input confining potential for the 2D Schrodinger equation.

For the numerical solution of the 3D-Poisson equation we use the standard 7-point finite difference approximation scheme in the presence of piecewise constant dielectric constants. This procedure leads to algebraic equations having a well defined structure, represented by matrix equation **Ax**=**b**. Dirichlet boundary conditions are implied at the Schottky contacts, whereas Neumann boundary conditions are assumed at the artificial boundaries. Within the incomplete factorization scheme [4] used for the solution of the 3D Poisson equation, the original matrix **A** is decomposed into a product of lower and upper triangular matrices **L** and **U**, respectively. This is achieved by modifying matrix **A** through the addition of a small matrix **N**. Thus, one solves the modified system **LUx**=**b**+**Nx** by solving successively the matrix equations **LV**=**b**+**Nx** and **V**=**Ux**, where **V** is an auxiliary matrix.

To obtain the spectrum given the potential, we solve a 2D finite difference Schrodinger equation with Dirichet boundary conditions. This yields a sparse matrix problem which we solve numerically by using ARPACK routines [5], which use Lanczos/Arnoldi factorization. Importantly, this method also allows for the computation of a subspace of eigenvectors, rather than the entire set, for a given matrix (typically, we are interested in only the lowest 100 eigenvalues). Using more standard methods for the eigenvalue problem leads to intractable storage and computational requirements.

3. HARD WALL RESULTS

Figure 2: Left panel, an eigenstate of a coupled dot system. Right panel, the confining potential and a classical orbit.

Before examining the results for potentials obtained self-consistently, we first consider the situation where confinement is achieved by an infinite potential well with vertical hard walls. While such a model is less realistic, the results are somewhat easier to interpret, since the dots can be clearly defined and made distinct from the QPCs connecting them. Fig. 2 illustrates the example of two circular dots connected by a QPC. On the left is the 88th eigenstate (in order of energy) of this coupled system. The individual circular dots here have radius 0.15 μm. Lighter shading corresponds to higher probability amplitude. The black region represents the model confining potential we have assumed. This eigenstate shows evidence of "scarring", that is, the amplitude appears to be maximized along a classical periodic orbit. The simplest classical trajectory that is a candidate for the orbit in question is the "hourglass" orbit shown in the right panel.

Fig. 3 shows eigenstates 66 through 90 of this system. States such as the 66th, 67th and 69th also show scarring, with triangular patterns not unlike that of the 88th state. That said, not all the states here show scarring effects we have singled out in the previous example. The wave function of 78th state for instance shows radial symmetry in each of the two dots, which is consistent with what one sees in individual dots. For comparison, the upper panel of Fig. 4 shows states 31 through 55 for a single circular dot. The 32nd state of the single dot system resembles what is occurring in the individual dots of the 78th state of the coupled system. There is a similar correspondence between state 85 of the coupled system and state 50 of the single dot system. That said, even in coupled dot states that do not show obvious scarring, there are states in which the radial symmetry of the single dots are obviously broken – for example, states 72 and 89.

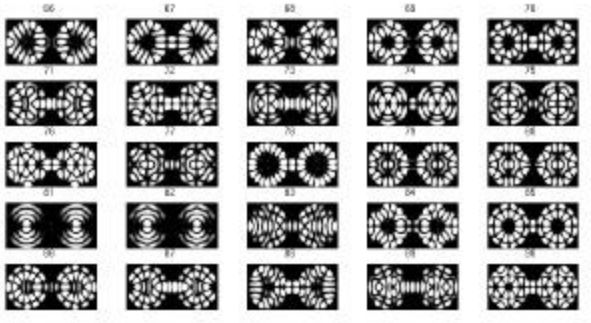

Figure 3: States 66 through 90 of the coupled dot system.

These results clearly show that when coupled by a QPC, two dots in series show a combination of behavior-coupled dot states that have strong single dot characteristics (eg. state 78) as well as states where the two dots truly act collectively as one unit (eg. state 72). A very important aspect of our results is that the two types of behavior are intermingled and there is no clear transition from single dot to collective behavior. In past work on coupled dot systems, it has been assumed that, once the QPC is wide enough that the electrons no longer have to tunnel between the two dots, the coupled system essentially behaves as if it were simply one large single dot. This is clearly not the case. It should be pointed out that the QPC that connects the two dots support 2

propagating modes for the energies of the states examined here, which is well beyond the tunneling regime.

In true molecules, the molecular states can be expressed as a linear combination of atomic states. Similarly, the coupled dot states shown here can be decomposed in terms of single dot states by means of vector projection. The right panel of Fig. 5 shows the result of a linear combination of single dot states that makes the best approximation in the right dot of the 88th coupled dot state shown in Fig. 2. The left panel shows the magnitude of the expansion coefficients of this linear combination. At least 5 single dot states make a major contribution – the 36th, the 40th , the 43rd , the 44th and the 50th . Clearly in the case of this scarred state, the coupling of the dots has resulted in a significant mixing of the single dot states. On the other hand, states such as the 78th discussed above have a dominant contribution from one single dot state.

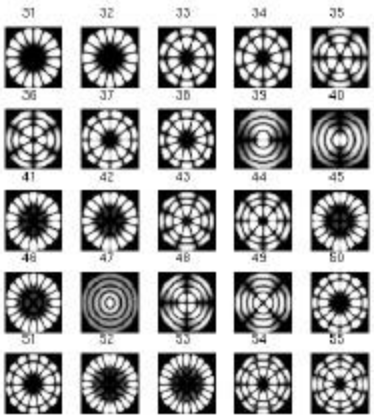

Figure 4: States 31 through 55 for a single dot.

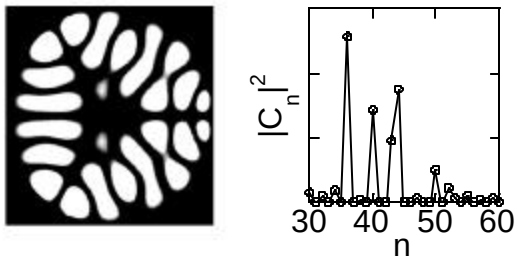

Figure 5: Left: the result of a linear combination of single dot states, right: the magnitude of the expansion coefficients.

What governs the scarring effects and the resulting mixing of single dot states? Obviously the geometry of the individual dots is an important factor. However just as important is the position of the QPCs coupling the dots. To illustrate this, we consider the case of two coupled square dots in Fig. 6. The top left panel shows the 107th state of a coupled square dot system in which the dots are 0.3 μm in size and the connecting QPC is at the top. On the top right is a classical periodic orbit that could be responsible for this scarring. As one might expect, no such state is possible in a circular dot system. If the position of the QPC is moved from the top edge of the dot to the middle, this classical orbit becomes disallowed. Consequently, the corresponding eigenstate vanishes. In this case, a new set of "molecular" eigenstates arises that are not possible in the original geometry. An example of this is shown in the bottom panel, which shows an eigenstate that has a crossing pattern.

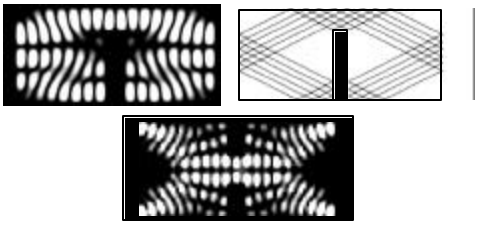

Figure 6: Upper right: a scarred coupled square dot eigenstate, upper right: the corresponding classical orbit, bottom: a different scarred state resulting from moving the QPCs.

4. SELF-CONSISTENT RESULTS

Figure 7: Three self-consistent potentials, corresponding to V_c = *-0.6, -1.0* and *–0.5V*, respectively.

We now present results for realistically modeled potentials obtained using the methods outlined in section 2. We consider the three examples illustrated in Fig. 7. These examples are distinguished by the voltage applied to the central gates, which are V_c = *-0.6, -1.0* and *–0.5 V,* respectively (all other gates are held fixed at *–1.0 V*). The darker the shading in these pictures, the lower the value of the potential. Note that the left panel corresponds to the same example illustrated in the bottom panel of Fig. 1. Comparing these three results, it is evident that changing V_c alters the amount of coupling between the two dots. However, it has another important effect : it changes the shape of the dots. For V_c = *-0.6* and *-1.0 V,* the individual dots are roughly circular in shape. In the V_c = *-0.5 V* case, the confining potential is somewhat more rectangular for each dot. In our previous section, we examined situations where the dots and the QPCs were well defined and readily distinguishable from one another. In the realistic situation, this is no longer the case. There is a smooth transition from dot to QPC, which now has the form of a "saddle". In this situation, it is now difficult to tell where a dot ends and a

QPC begins. This makes it difficult to unambiguously apply the analysis of the previous section to these realistic dots.

Fig. 8 shows eigenstates 61 to 80 for the $V_c = -0.6\ V$ states. The results here are somewhat similar to those shown for the perfectly circular dots in Fig. 3. In particular, the central "bar" feature evident in states 63 and 64 are quite reminiscent to what is shown in state 73 of Fig. 3. One also sees similar "quasi-atomic" states. On the other hand, the triangular patterns shown in the "scars" of the coupled circular dots do not show up here. This is a testament to the fact that these dots are only approximately circular. Only truly circular dots will support these particular scarring patterns.

In the bottom two panels of Fig. 8, we show close-ups of eigenstates 61 and 62. These are quite similar, both scarred perhaps by an orbit similar to the "hourglass" discussed in the context of Fig. 3, except here the orbit forms a diamond shape rather than triangular in each dot. These two states are interesting for another reason. State 61 has a peak in quantum mechanical amplitude in the middle of the QPC. On the other hand, the higher energy state, 62, has a minimum in amplitude in this very same location. This is analogous to the situation in molecules, where bonding states, which are lower in energy, have significant amplitude in between the atoms, while the higher energy anti-bonding states have their amplitude go to zero at the midpoint between atoms.

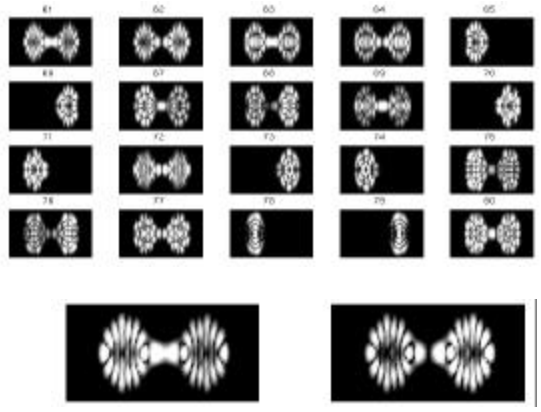

Figure 8: Upper panel: states 61 through 80 of the $V_c = -0.6V$ system, lower left panel: a close-up of state 61, lower right: state 62.

For comparison, Fig. 9 shows eigenstates 61 through 80 for the $V_c = -1.0\ V$ system. As one might expect, at this higher gate voltage, the QPCs are pinched off enough so that the two dots in the system appear to be virtually uncoupled, at least at the energies corresponding to these eigenstates. In regards to this, the amplitude of each state is peaked in only one dot at a time, and the states appear in quasi-degenerate pairs. That said, even in this case, there is still enough coupling to split energy levels. Note that state 70 is separated in energy from its mirror twin, state 75, by 4 other eigenstates. If there were no coupling, these two states should have appeared in sequence.

Finally, in Fig. 10, we show two eigenstates from the $V_c = -0.5\ V$ system. As expected, these states reflect the more rectangular geometry generated by this applied voltage. These two states also show a different scarring pattern not evident in the previous geometries, forming a "V" in each dot. Here again, we see a "bonding" and "anti-bonding" pair of states.

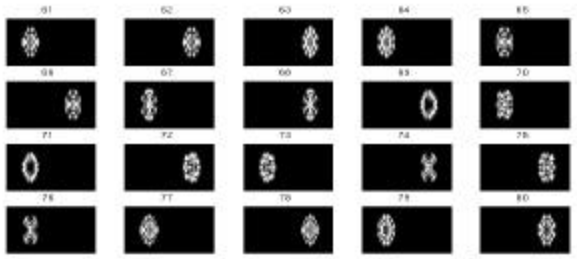

Figure 9: States 61 through 80 of the $V_c = -1.0\ V$ system.

Figure 10: States 105 and 106 of the $V_c = -0.5\ V$ system.

6. CONCLUSIONS

Regarding coupled quantum dots, we have found that they indeed can behave like artificial molecules. In particular, we have found what appear to be bonding and anti-bonding states. We have also found that there is no simple crossover from "atomic" to "molecular" behavior and that the classical behavior of the system can determine in many cases the resulting quantum mechanical states.

REFERENCES

* The authors would like to acknowledge the financial support from NSF and ONR.

[1] M. A. Kastner, Rev. Mod. Phys. 64, 849 1992.

[2] See F. Ramirez, E. Cota and S. E. Ulloa, Phys. Rev. B, 59, 5717 (1999) and references therein.

[3] R. Akis, D. Vasileska, D. K. Ferry, J.P. Bird, Y. Okubo, Y. Ochiai, K. Ishibashi, Y. Aoyagi, and T. Sugano, Physica B 249-251, 368 (1998).

[4] G. V. Gadiyak and M. S. Obrecht, in *Simulation of Semiconductor Devices and Processes: Proceedings of the Second International Conference*, Ed. by K. Board and D. R. J. Owen, Swansea UK (Pineridge Press, 1986).

[5] website:http://www.caam.rice.edu/software/ARPACK/index.html .